Minimal model for tumor angiogenesis

P. G. Kevrekidis,[1] N. Whitaker,[1] D. J. Good,[2] and G. J. Herring[1]
[1]*Department of Mathematics and Statistics, University of Massachusetts, Amherst, Massachusetts 01003-4515, USA*
[2]*Department of Veterinary and Animal Sciences, University of Massachusetts, Amherst, Massachusetts 01003-4515, USA*
(Received 20 June 2005; revised manuscript received 5 April 2006; published 30 June 2006)

In this work, we show a mathematical model for the angiogenesis by endothelial cells. We present the model at the level of partial differential equations, describing the spatiotemporal evolution of the cell population, the extracellular matrix macromolecules, the proteases, the tumor angiogenic factors, and the possible presence of inhibitors. We mainly focus, however, on a complementary, more physiologically realistic, hybrid approach in which the cells are treated as individual particles. We examine the model numerically in two-dimensional settings, discussing its comparison with experimental results.

DOI: 10.1103/PhysRevE.73.061926 PACS number(s): 87.17.Aa

I. INTRODUCTION

Angiogenesis is the process of formation of capillary cellular sprouts in response to external chemical stimuli, leading eventually to the formation of blood vessels. It is relevant to the formation of the placenta during embryogenesis [1], the repair of mammalian tissue following injury [2] but, more importantly for the purposes of the present study, to the process of tumor growth.

In the last decade, an increasing effort has been made to mathematically describe the dynamical evolution of angiogenesis and its role in tumor growth. Principally, this effort is centered around modeling the proliferation of endothelial cells towards the tumor, as they are attracted by the tumor angiogenic factors (TAFs) [3] in the background of the extracellular matrix (ECM) [4]. A number of studies examine the role of the proteases secreted by the tumor that induce degradation of the ECM and, hence, directed motion of the endothelial cells towards the tumor [5]. Other models only consider the cell population evolution and its coupling to the ECM [6]. Similar models have been proposed for the study of tumor growth, coupled to the presence of nutrients, see e.g., [7,8]. Finally, much more complicated, multispecies models with detailed chemistry have also been proposed such as, e.g., the nine species models of [9].

Our aim here is to revisit this problem from the perspective of deriving a "minimal" model that includes the principal biological interactions that contribute to the vascularization of the cancerous tissue. A more specific goal is to use the resulting model to reproduce qualitatively *in vivo* experiments of angiogenesis such as, e.g., the ones of Ref. [10]. Notice that our viewpoint of the problem is quite similar to the one of the recent works of Refs. [11–15], even though the model and the principal processes it examines are to a considerable extent different.

While most of the above mentioned theoretical works are formulated in the continuum limit of description through concentration fields (see also [16,17]), others have advocated the use of discrete particle simulations [4] with a set of transition probabilities for one-step cell jumps. The latter class of models can be systematically derived from their continuum siblings (in the spirit of [18]; see also [19]) and are equivalent to the former as the limit is approached. In the present work, we follow the latter particle method. Thus, while we originally set up the problem at the continuum, partial differential equation (PDE) level, we present and advocate the systematic use of a particle formulation.

Our presentation will be structured as follows: in Sec. II, we present the main biological mechanisms, and how they can be translated, through physical intuition, into a minimal mathematical model based on a PDE formulation. In Sec. III, we present a corresponding particle based model that is based on the PDE and incorporates these mechanisms. In Sec. IV, we numerically study the model in two spatial dimensions. Finally, in Sec. V, we summarize our findings and present a number of interesting extensions for future studies.

II. PHYSICAL MECHANISMS AND PDE MODEL

During angiogenesis, endothelial cells proliferate and form a capillary sprout network in response to the TAF stimuli secreted by the tumor. As a result the cells eventually vascularize the tumor leading to its growth. Their motion occurs in the ECM substrate where they interact with macromolecules, such as fibronectin. The attraction of cells to ECM gradients (termed "haptotaxis" [4]) prevents them from approaching the tumor. Furthermore, the cells, and predominantly the tumor secrete proteases (P) that degrade the ECM, assisting angiogenesis. Finally, when protease is generated, the fibroblast cells in the ECM generate inhibitors (I) that will, in turn, inactivate the protease, as well as inhibit the cell motion towards the tumor; additional functions of the inhibitors such as their enhancement of cell death [20] occur over longer time scales and will be ignored here. Hence, there are five principal "species" that should naturally be included in a biologically relevant and physically motivated, mathematical model of angiogenesis, namely the cells (C), the TAFs (T), the extracellular matrix proteins such as fibronectin (F), the proteases (P), and the inhibitors (I). For each of these species, we summarize their principal role in the angiogenesis process, as follows:

(i) The cells: they diffuse (migrate) in the ECM, get generated (mitogenesis or proliferation), and die (apoptosis). They are driven to the TAF concentration gradients (chemotaxis) [4], as well as towards ECM concentration gradients [4,5] and are similarly "repelled" from inhibitor gradients

[10]. Hence, the dynamics that we will use for the evolution of the cell will be similar to the one proposed by [4], but for the inclusion of the relevant inhibitor term.

(ii) The TAFs: for these, one can consider, in principle, processes of their uptake by the ECM as well as processes (over longer periods of time) of their random secretion by the tumor. However, for the purposes of the present work (i.e., for the shorter time scales of the order of a few days considered here), we will assume the TAF concentration as being fixed (i.e., at a steady state; see also [4]).

(iii) The ECM: the secretion of proteases by the tumor gradually degrades the ECM; proteases involved in the angiogenic process (such as metalloproteases) bind to the macromolecules of the ECM, depleting it, and hence allowing the cells to be driven to the tumor. The relevant evolution equation here is motivated by [4], however, it is appropriately modified to account for the source of degradation in a more physiologically realistic manner. In addition, we should note here that in comparison with the surrounding ECM components, the fibronectin has a large molecular weight making diffusion slow and difficult. In addition, fibronectin is bound to the surrounding ECM by noncovalent links. As a result, the diffusivity of the fibronectin is small enough that it will be ignored for the purposes of this paper.

(iv) The proteases: during angiogenesis, there are many sources of protease production and our model incorporates two of these: secretion of proteases by the tumor (i.e., predominantly in the vicinity of regions where the TAF concentration is high) and proteases created through the interaction of the endothelial cells with the TAFs. After secretion, the proteases are free to diffuse throughout the ECM where they either bind to the endothelial cell surface for use in breaking down the fibronectin, or bind to components of the ECM, or become inactivated by protease inhibitors. Notice that the natural, self-degradation of the protease can also be easily included in the model, even though it will be neglected here.

(v) The inhibitors: their diffusion will be neglected, but their mutual neutralization with the proteases will be accounted for. As noted in [10], as well as in other experiments using concentrated pellets of inhibitor (in an artificial system), the diffusion of the inhibitor can be inferred as being negligible in the time scale of the assay. Secondly, *in vivo*, inhibitors such as thrombospondin (TSP) bind to ECM molecules such as collagen, heparin, and fibronectin [21–23], and this limits the diffusion because the molecule is held in place by the ECM through these interactions. Instead, the principal role of the inhibitor is to block angiogenic growth towards the pellet.

It is then natural to set up a five "species" dynamical evolution model as follows:

$$C_t = D_c \Delta C - \nabla \cdot (f_F \nabla F) - \nabla \cdot (f_T \nabla T) + \nabla \cdot (f_I \nabla I) + k_1 C(1-C), \quad (1)$$

$$F_t = -k_2 PF, \quad (2)$$

$$P_t = D_P \Delta P - k_3 PI + k_4 TC + k_5 T, \quad (3)$$

$$I_t = -k_3 PI. \quad (4)$$

The fifth species in the model of Eqs. (1)–(4) is the TAF concentration T that will be described in detail below. The diffusion coefficient of the cells is taken to be $D_c = 0.000\,35$, following the spatial and temporal scaling of [4]. In particular, the relevant motility coefficients in dimensional units are in the range of $D_c = 10^{-10}$ cm^2/sec. This estimate is based on the cell migration experiments of [24,25] (however, when the cells migrate in the presence of neighbors, this may be an overestimate; see e.g., the discussion of [26]). It is also important to note that the nondimensionalization of the equations follows the discussion of [4], using 2 mm as the relevant (unit) length scale and 1.5 days as the relevant (unit) time scale. The terms containing f_T, f_F, and f_I represent, respectively, the chemotactic attraction of the cells towards the tumor, the haptotactic response to the ECM gradients such as fibronectin, and the "repulsive" effect of inhibitor gradients (notice the opposite sign in the latter). Following, in part, the estimates of [4] whose model includes T and F, we use $f_F = a_1 C$ and $f_T = a_2 C/(1 + a_3 T)$ (where the latter assumes chemotactic sensitivity decreases as TAF concentration increases, see also [27]). Similarly, we use $f_I = a_4 C$. The relevant functions are proportional to the cell concentration C, as they should according to the intuition that "-tactic" terms demonstrate the attraction of the endothelial cells to the corresponding gradients. For most parameters, we adopt the estimates of Ref. [4]. We comment below on the terms that are absent in the latter model. For our intensive two-dimensional (2D) computations, we use a domain of $[0,1] \times [0,1]$, with a TAF profile of $T = \exp(-r^2/\epsilon)$ where r is the distance from the center of the tumor and $\epsilon = 0.45$. Based upon the molecular size of the proteases, we estimated their diffusivity to be $\approx 10^{-6} - 10^{-7}$ cm^2/sec, resulting in a nondimensional protease diffusion rate of $D_P \approx 1$. The inhibitors were absent in most previous models, however, in order for them to produce *in vivo* results similar to the ones displayed in Fig. 3 of [10], the strength of their "repulsion" should be comparable to the TAF attraction. We use these *in vivo* experiments as a qualitative guide for the validation of our model. The last term in Eq. (1) reflects the proliferation of cells, incorporating both cell generation and apoptotic components. In Eq. (2), the term on the right-hand side represents the annihilation of the fibronectin due to the protease. In Eq. (3), the first term represents diffusion of the protease, the second term represents the annihilation of the protease due to its binding with the inhibitors, the third term represents the growth of protease due to the interaction of the cells with the TAFs, and the last term represents the generation of protease where TAF concentration is high. Finally, in Eq. (4), the inhibitors are depleted due to their interaction with the protease. Lastly, we have not been able to identify in the literature the remaining parameter values, thus values of $k_2 = k_3 = k_4 = 0.1$ and $k_5 = 0.2$ are chosen as typical values (we have found them to be representative of the relevant phenomenology).

III. PARTICLE MODEL

While the continuum model is valuable in revealing some of the phenomenology and helpful in modeling mathemati-

cally each of the physically relevant processes, it is clear that a discrete, particlelike model would be much closer in practice to a physiological experiment. In the spirit of comparison with direct *in vitro* or *in vivo* experiments that monitor the development of the sprout network, it is natural to formulate a model for the propagation of a single cell (at the tip of a forming sprout) rather than a continuum distribution of cell density. In order to generate such a model, we build and expand on the method of Ref. [4], based on the transition probability formulation of Ref. [18]. The latter, by construction, incorporates the "correct" continuum limit. In order to develop this approach, one can consider a simple, explicit Euler, centered-difference scheme for the solution of Eqs. (1)–(4). The corresponding "lattice" equation for the endothelial cells (in one spatial dimension) can be rewritten as follows:

$$C_n^{k+1} = P_r C_{n-1}^k + P_s C_n^k + P_l C_{n+1}^k, \tag{5}$$

where:

$$P_s = 1 + \Delta t\left[-2\frac{D_c}{\Delta x^2} - a_1 \Delta_2 F_n^k \right] - \frac{a_2 \Delta t}{1 + a_3 T_n^k} \Delta_2 T_n^k + a_4 \Delta t \Delta_2 I_n^k + k_1(1 - C_n^k), \tag{6}$$

$$P_r = \Delta t\left[\frac{D_c}{\Delta x^2} + a_1 \frac{F_{n+1}^k - F_{n-1}^k}{4\Delta x^2} \right] + \frac{a_2 \Delta t}{1 + a_3 T_{n-1}^k} \frac{T_{n+1}^k - T_{n-1}^k}{4\Delta x^2} - a_4 \Delta t \frac{I_{n+1}^k - I_{n-1}^k}{4\Delta x^2}, \tag{7}$$

$$P_l = \Delta t\left[\frac{D_c}{\Delta x^2} - a_1 \frac{F_{n+1}^k - F_{n-1}^k}{4\Delta x^2} \right] - \frac{a_2 \Delta t}{1 + a_3 T_{n+1}^k} \frac{T_{n+1}^k - T_{n-1}^k}{4\Delta x^2} + a_4 \Delta t \frac{I_{n+1}^k - I_{n-1}^k}{4\Delta x^2}, \tag{8}$$

where $\Delta_2 Q_n^k = (Q_{n+1}^k + Q_{n-1}^k - 2Q_n^k)/\Delta x^2$ is the discrete Laplacian; furthermore $C_n^k \equiv C(n\Delta x, k\Delta t)$ represents the discretization of the continuum field $C(x,t)$, Δx and Δt are the corresponding spatial and temporal steps.

This can then be considered as a probabilistic model in the following biased random walk sense: the term proportional to C_n^k, yields the "contribution" to C_n^{k+1} from C_n^k. Hence, if appropriately normalized, it denotes the probability that the cell will *remain* in the same position at the next time step. On the other hand, the term proportional to C_{n+1}^k denotes the contribution to C_n^{k+1} from its right neighbor, hence if normalized, it amounts to the probability of moving to n from $n+1$, i.e., of moving to the left. Similarly, the term $\propto C_{n-1}^k$ can be normalized to the probability of moving to the right. The natural normalization factor is given by the sum of the probabilities. Upon normalization, we use a (uniformly distributed) random number generator to infer (by comparing with the relevant probabilities P_r, P_s, and P_l) whether the particle will move to the right, stay on the same location or move to the left.

Notice that by construction, this probabilistic formulation emulates the PDE description at the level of a particle simulation. Furthermore, it is important to note that while we gave the one-dimensional (1D) formulation for simplicity, the same steps can be straightforwardly implemented in 2D, using the relevant five-point stencil, and including probabilities for moving up, down, left, right, as well as for staying at the same site. The corresponding probabilities in this case are given by:

$$P_s = 1 - \Delta t\left[2\frac{D_c}{\Delta x^2} + 2\frac{D_c}{\Delta y^2} - a_1 \Delta_2 F_{n,m}^k \right] - \frac{a_2 \Delta t}{1 + a_3 T_n^k} \Delta_2 T_{n,m}^k + a_4 \Delta t \Delta_2 I_{n,m}^k + k_1(1 - C_n^k), \tag{9}$$

$$P_r = \Delta t\left[\frac{D_c}{\Delta x^2} + a_1 \frac{\Delta_x F_{n,m}^k}{2\Delta x} \right] + \frac{a_2 \Delta t}{1 + a_3 T_{n-1,m}^k} \frac{\Delta_x T_{n,m}^k}{2\Delta x} - a_4 \Delta t \frac{\Delta_x I_{n,m}^k}{2\Delta x}, \tag{10}$$

$$P_l = \Delta t\left[\frac{D_c}{\Delta x^2} - a_1 \frac{\Delta_x F_{n,m}^k}{2\Delta x} \right] - \frac{a_2 \Delta t}{1 + a_3 T_{n+1,m}^k} \frac{\Delta_x T_{n,m}^k}{2\Delta x} + a_4 \Delta t \frac{\Delta_x I_{n,m}^k}{2\Delta x}, \tag{11}$$

$$P_u = \Delta t\left[\frac{D_c}{\Delta y^2} + a_1 \frac{\Delta_y F_{n,m}^k}{2\Delta y} \right] + \frac{a_2 \Delta t}{1 + a_3 T_{n-1}^k} \frac{\Delta_y T_{n,m}^k}{2\Delta y} - a_4 \Delta t \frac{\Delta_y I_{n,m}^k}{2\Delta y}, \tag{12}$$

$$P_d = \Delta t\left[\frac{D_c}{\Delta y^2} - a_1 \frac{\Delta_y F_{n,m}^k}{2\Delta y} \right] - \frac{a_2 \Delta t}{1 + a_3 T_{n+1}^k} \frac{\Delta_y T_{n,m}^k}{2\Delta y} + a_4 \Delta t \frac{\Delta_y I_{n,m}^k}{2\Delta y}, \tag{13}$$

where $\Delta_2 Q_{n,m}^k = (Q_{n+1,m}^k + Q_{n-1,m}^k - 2Q_{n,m}^k)/\Delta x^2 + (Q_{n,m+1}^k + Q_{n,m-1}^k - 2Q_{n,m}^k)/\Delta y^2$ is the discrete Laplacian and $\Delta_x Q_{n,m}^k = (Q_{n+1,m}^k - Q_{n-1,m}^k)/2\Delta x$ and $\Delta_y Q_{n,m}^k = (Q_{n,m+1}^k - Q_{n,m-1}^k)/2\Delta y$ are the discrete first derivatives in x and y, respectively. Additionally $C_{n,m}^k \equiv C(n\Delta x, m\Delta y, k\Delta t)$ represents the discretization of the continuum field $C(x,y,t)$: Δx, Δy, and Δt being the corresponding spatial and temporal steps.

It should also be mentioned that in this formulation, the original model assumes a hybrid form wherein the particle simulation is solved on the same grid as the PDEs for the remaining four species (F, T, P, and I). There are a number of modifications of the above adjustment of the methodology of [4] in our numerical implementation of the particle simulation, such as, e.g., our inclusion of concentration dependent terms, absent in [4]. In particular, the concentration field can be assigned in a binary form in this particle setting: $C_n^k = \delta_{n,x_0}$, where x_0 is the location of the cell(s) and δ stands for the Kronecker δ. Notice that the relevant terms principally include the stochasticity coming from the movement, even though the contribution of proliferation/apoptosis is also incorporated in the relevant expression for P_s.

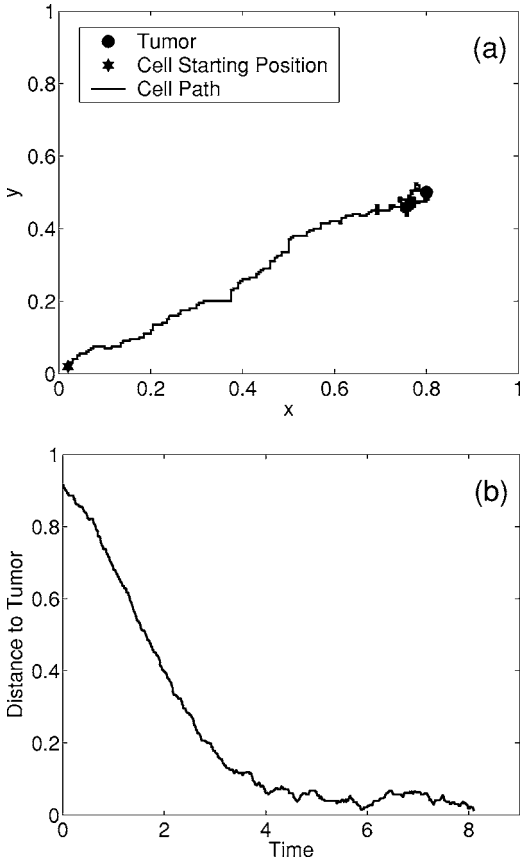

FIG. 1. The 2D case without the inhibitor. The left panel shows the motion of the cell (solid line showing the motion of the sprout tip) towards the tumor (dot). The right panel shows the distance of the sprout tip from the tumor center. Already for $t \approx 6$, the cell has arrived at the tumor.

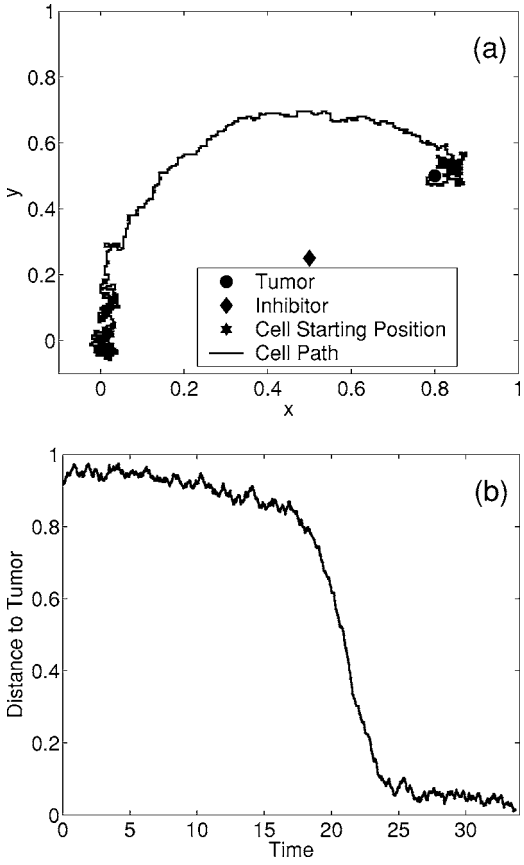

FIG. 2. Same as the previous figure, but in the presence of an inhibitor centered around $(0.5, 0.25)$. The path can be approximated by a circular arc with center located at the inhibitor and of radius 0.49.

In summary, the behavior of a capillary sprout is calculated by modeling the movement of the sprout's leading endothelial cell via a biased random walk. At each time step, probability ranges are calculated by normalizing the results of Eqs. (9)–(13): stay range $=0-P_s/P_{total}$, move left range $=P_s/P_{total}-(P_s+P_l)/P_{total}$, move right range $=(P_s+P_l)/P_{total}-(P_s+P_l+P_r)/P_{total}$, etc., where:

$$P_{total} = P_s + P_l + P_r + P_u + P_d. \tag{14}$$

The cell's movement is then determined by comparing a random number (uniformly distributed between 0 and 1) with the probability ranges above.

We hereafter focus on the main numerical findings of the above model and their qualitative comparison with the experiments of [10].

IV. NUMERICAL RESULTS

We now give a number of typical numerical results. We focus our attention, for the purposes of the present work, on the physiologically realistic 2D case. Our findings are summarized in Figs. 1–4 for the cells (as well as in Fig. 5 showing the T, F, P, and I fields that are coupled to the cells in our simulations). The ECM fibronectin is initialized using a uniformly distributed random profile. The protease is initialized in a similar way, but biased towards the tumor (numerically achieved through multiplying its random distribution by that of the TAFs). This is due to the fact that the proteases are predominantly secreted by the TAFs and, hence, will most likely exist in regions where the TAF concentration is maximal.

Figure 1 shows the case of a particle realization approaching the tumor center located at $(x,y)=(0.8,0.5)$. Clearly, already at short times of the order of $t \approx 6$, in this case where the inhibitor is absent, the cell has "arrived" at the location of the tumor. This result is typical for this case: an average "arrival" time of 6.6 [1.6186 standard deviation (STD)] was calculated with 25 runs using the same initial conditions. Also calculated was the average length of the pattern formed. This was measured by the number of times the cell moved during the simulation multiplied by the grid size (≈ 10 μm). For this case, the average length was 3.25 mm. In Fig. 2 we perform an intermediate–inhibitor experiment, motivated by the studies of [10]: in the latter, the adhesive glycoprotein thrombospondin (TSP) was used in a pellet (alongside an inducer) to prevent the capillary sprout neovascularization of corneas. Similar functions were demonstrated, in experiments *in vitro*, by the hamster protein gp140, a proteolytic fragment of TSP. Here, we place a localized inhibitor concentration between the cell initial position and the tumor [the

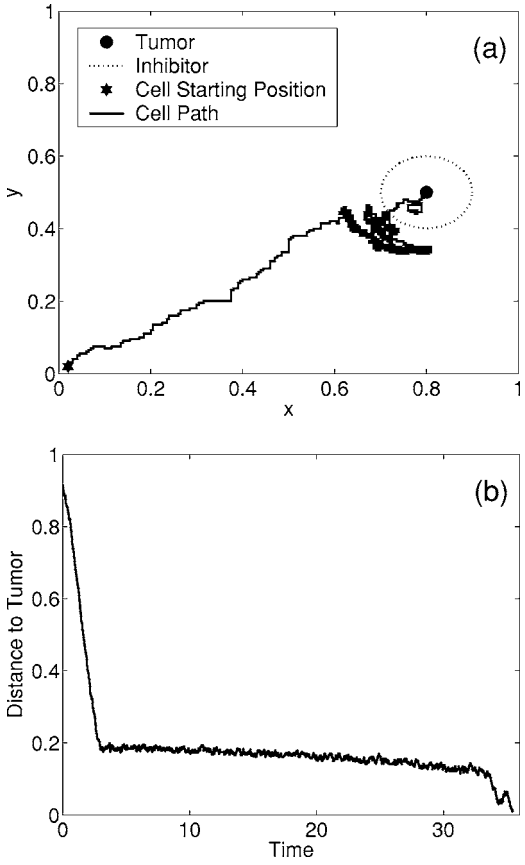

FIG. 3. Same as the previous figures but for an inhibitor ring initially around the tumor (see text for details).

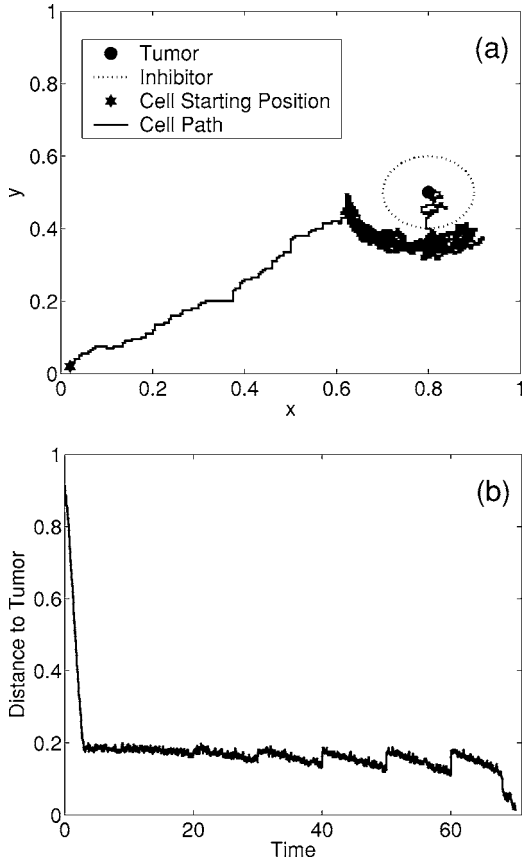

FIG. 4. This is essentially the same as the previous figure except that the inhibitor is replenished every ten time units.

inhibitor I is centered around $(x,y)=(0.5,0.25)$]. In this case, interestingly, the cell takes advantage of the geometry in order to reach the tumor. In particular, it takes a longer time to arrive at the tumor [in comparison with Fig. 1, i.e., here the arrival time is ≈ 34, with an average time of 33.08 (3.2291 STD) and average length of 9.38 mm over 10 runs] but eventually the cell circumvents the inhibiting obstacle and finds its way towards the tumor center[1]. The trajectory appears to follow the arc of a circle. Starting soon after initialization, the average distance from points on the trajectory to the inhibitor were calculated to be 0.49. The arc of a circle of radius 0.49 with center $(0.5,0.25)$ closely fits the path of the cell. Figure 3 more closely emulates the experiment of [10]: we place a localized "chunk" of inhibitor in a thin ring around the tumor center $\{I \sim \mathrm{sech}[100*(r-0.1)]$, where r is the distance from the tumor$\}$. In this case, the cell arrives close to the tumor for $t \approx 3$, but is prevented by the inhibitor "layer" to get any closer and hence "wanders" in the vicinity of the inhibitor ring until $t \approx 35$ [average time 35.32 (0.8550 STD) and average length 8.84 mm over 10 runs], when the inhibitor concentration is practically extinguished due to its interaction with P, and then the cell finally arrives at the tumor. Finally, in Fig. 4, all conditions are the same as in Fig. 3 except that the inhibitor is replenished to its initial value every ten time units. At approximately 30 time units, the inhibitors would normally be depleted and the cells would begin to propagate as shown in our time versus distance plot. This experiment indicates that tumor growth could be controlled and possibly prevented through the periodic replenishment of the inhibitor. The example clearly illustrates the delay effect due to the inhibitor presence in the angiogenesis process due to the periodic increase of the inhibitor strength. Furthermore, we should note that the results demonstrated here were found to be *generic* and representative of the different regimes of the absence and of the presence of the inhibitor.

V. CONCLUSIONS

In this work, we presented a mathematical model for angiogenesis, aiming at a minimal description incorporating the key biological populations and consonant with *in vitro* and *in vivo* experiments such as the ones of Ref. [10]. We have included the population of the inhibitors in the model and demonstrated that it can play a critical role in delaying and possibly even preventing angiogenesis (if periodically repeated, targeted doses of inhibitor pellets are provided). Clearly, this first step can be ramified in a number of different directions. Citing a few of them, we mention: the inclusion of dynamics for the inducers which have been assumed

[1]Due to the strength of the inhibitor and usage of no-flux boundary conditions, the bottom and left boundaries of the domain were moved 0.1 units in order to allow the cell to freely move.

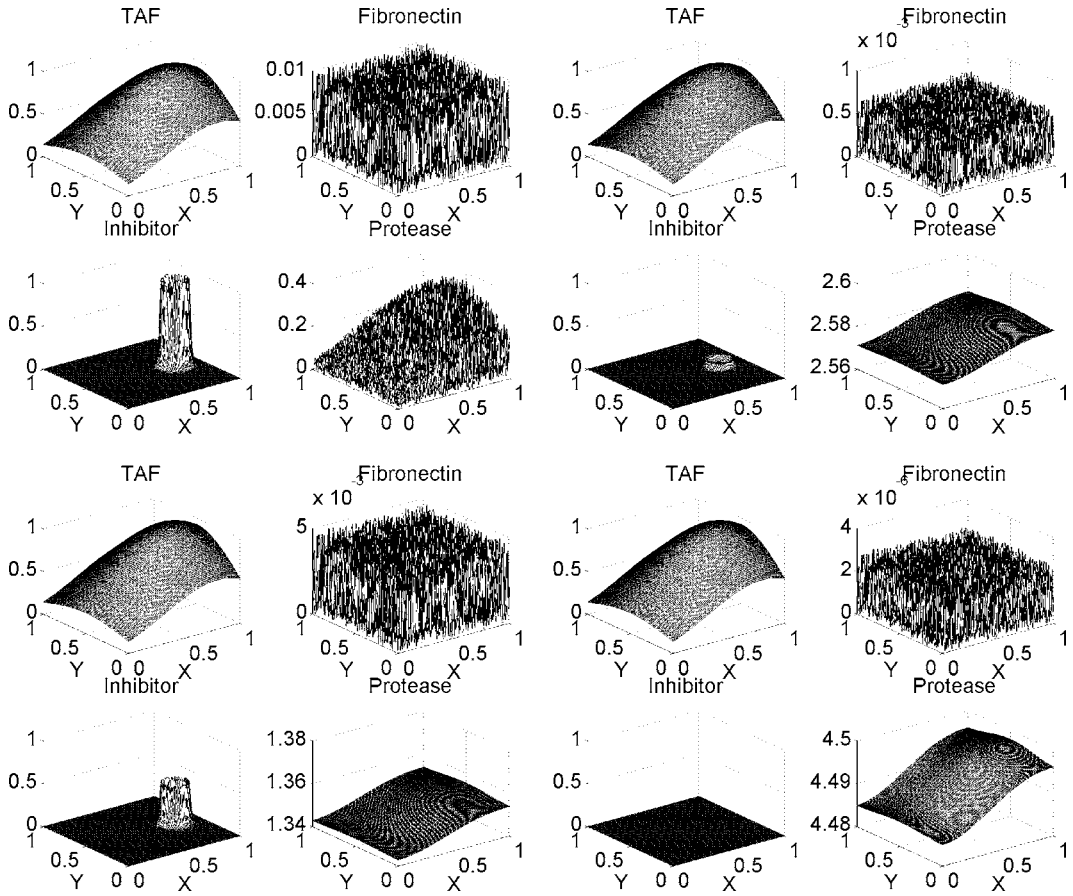

FIG. 5. This panel shows the concentration of T, F, I, and P at $t=0$ (top left panels), $t=10$ (top right panels), $t=20$ (bottom left panels), and $t=35.48$ (bottom right panels) for Fig. 3.

here at steady state (this is relevant particularly for studies of longer time scales); the relevance of ECM and inhibitor dependences of the coefficients governing cell proliferation that has recently been demonstrated experimentally [28,29].

More detailed interactions (diffusion of I, degradation of P, generation of I from the fibroblast cells and diffuse rather than localized concentration of the latter, etc.) can also be incorporated. However, we believe that the present model captures the qualitative basis of angiogenesis of endothelial cells and can be used as a building block toward a more quantitative understanding of the phenomenon. It can potentially serve as a protocol devising strategy for inhibiting angiogenesis. One such example was discussed in Fig. 4. In particular, our model predictions illustrated that there is a critical time (e.g., in the setting of Fig. 3, $t_{cr} \approx 30$), beyond which the inhibitor is inactivated by the protease and hence the cells vascularize the tumor. Thus, if the inhibitor concentration is periodically "replenished" for a time close to the critical time, then it may become possible to delay and possibly even completely inhibit the angiogenesis process, thus eventually inducing tumor death. A numerical experiment illustrating this principle is shown in Fig. 4.

Another useful aspect of the model is that it can be used as a reverse-engineering technique for inferring some of the dependences that cannot be measured directly such as, e.g., the strength of the attraction of the cells to ECM (or other) gradients. Such aspects of the model are currently under investigation and will be reported in future work.

[1] C. H. Graham and P. K. Lala, Biochem. Cell Biol. **70**, 867 (1992).
[2] F. Arnold and D. C. West, Pharmacol. Ther. **52**, 407 (1991).
[3] J. Folkman and M. Klagsbrun, Science **235**, 442 (1987).
[4] A. R. A. Anderson and M. A. J. Chaplain, Bull. Math. Biol. **60**, 857 (1998).
[5] A. J. Perumpanani and J. Norbury, Math. Comput. Modell. **30**, 123 (1999).
[6] L. Olsen, J. A. Sherratt, and P. K. Maini, IMA J. Math. Appl. Med. Biol. **14**, 261 (1997).
[7] L. M. Sander and T. S. Deisboeck, Phys. Rev. E **66**, 051901 (2002).
[8] M. Scalerandi, B. Capogrosso Sansone, C. Benati, and C. A. Condat, Phys. Rev. E **65**, 051918 (2002).
[9] H. A. Levine, A. L. Tucker, and M. Nilsen-Hamilton, Growth Factors **20**, 155 (2002).

[10] D. J. Good, P. J. Polverini, F. Rastinejad, M. M. Le Beau, R. S. Lemons, W. A. Frazier, and N. P. Bouck, Proc. Natl. Acad. Sci. U.S.A. **87**, 6624 (1990).
[11] M. Scalerandi, A. Romano, G. P. Pescarmona, P. P. Delsanto, and C. A. Condat, Phys. Rev. E **59**, 2206 (1999).
[12] P. P. Delsanto, A. Romano, M. Scalerandi, and G. P. Pescarmona, Phys. Rev. E **62**, 2547 (2000).
[13] B. Capogrosso Sansone, M. Scalerandi, and C. A. Condat, Phys. Rev. Lett. **87**, 128102 (2001).
[14] M. Scalerandi, B. C. Sansone, and C. A. Condat, Phys. Rev. E **65**, 011902 (2001).
[15] M. Scalerandi and F. Peggion, Phys. Rev. E **66**, 031903 (2002).
[16] A. J. Perumpanani, J. A. Sherratt, and J. Norbury, Nonlinearity **10**, 1599 (1997).
[17] H. M. Byrne and M. A. J. Chaplain, Bull. Math. Biol. **57**, 461 (1995).
[18] H. Othmer and A. Stevens, SIAM J. Appl. Math. **57**, 1044 (1997).
[19] S. R. McDougall, A. R. A. Anderson, M. A. J. Chaplain, and J. A. Sherratt, Bull. Math. Biol. **64**, 673 (2002).
[20] See, e.g., B. Jimenez *et al.*, Nat. Med. **6**, 41 (2000).
[21] R. Dardik and J. Lahav, Exp. Cell Res. **248**, 407 (1999).
[22] R. Dardik and J. Lahav, Eur. J. Biochem. **185**, 581 (1989).
[23] J. Takagi, T. Fujisawa, T. Usui, T. Aoyama, and Y. Saito, J. Biol. Chem. **268**, 15544 (1993).
[24] C. L. Stokes, M. A. Rupnick, S. K. Williams, and D. A. Lauffenburger, Lab. Invest. **63**, 657 (1990).
[25] M. A. Rupnick, C. L. Stokes, S. K. Williams, and D. A. Lauffenburger, Lab. Invest. **59**, 363 (1988).
[26] D. Bray, *Cell Movements* (Garland Publishing, New York, 1992).
[27] J. A. Sherratt, Bull. Math. Biol. **56**, 129 (1994).
[28] E. Chavakis and S. Dimmeler, Arterioscler., Thromb., Vasc. Biol. **22**, 887 (2002).
[29] S. Kim, M. Bakre, H. Yin, and J. A. Varner, J. Clin. Invest. **110**, 933 (2002).